Energy Conversion and Management 94 (2015) 19–27

Contents lists available at ScienceDirect

Energy Conversion and Management

journal homepage: www.elsevier.com/locate/enconman

Assessment of the adsorber surface density influence on the performance and operation of the intermittent SAR system

H.Z. Hassan *

Department of Mechanical Engineering, College of Engineering, Alfaisal University, Takhassusi St. P.O. Box 50927, Riyadh 11533, Saudi Arabia

ARTICLE INFO

Article history:
Received 6 October 2014
Accepted 21 January 2015

Keywords:
Adsorption cooling
Solar energy
Silica gel
Surface density
Water cooler
Dynamic simulation

ABSTRACT

The adsorber surface density is a chief factor which is strongly coupled with other design parameters and climate conditions. This parameter has a considerable impact on the behaviour and operation of the intermittent solar adsorption refrigeration (SAR) system. This paper presents a theoretical investigation of the impact of the adsorption reactor surface density on the behaviour and overall performance indices of the intermittent SAR system. A water chiller which uses silica gel and water adsorption pair is studied under the climate conditions of Riyadh. The mathematical model is developed and a computer program is constructed to run the dynamic simulation of the chiller. Results obtained from the study show that the studied water chiller will fail to complete the cycle and to produce a cooling effect when the surface density is greater than 44 kg/m^2. Moreover, the coefficient of performance (COP) increases with decreasing the surface density. Additionally, the optimum solar-to-cold conversion factor attains a value of 0.2 corresponding to surface density of 12.6 kg/m^2 and COP of 0.43. This shows that the COP is not the accurate gauge for the SAR system performance and the solar-to-cold conversion factor is suggested when evaluating SAR system performance.

© 2015 Elsevier Ltd. All rights reserved.

1. Introduction

Cooling and refrigeration processes are chief requisites and vital requirements for human beings today. Cold generating machines contribute mostly to the drink and food preservation industry manufacturing processes and control of the environment, to name a few. Much more of the world's generated electrical energy is directed to power the traditional vapour compression cooling systems especially for environmental control in countries with warm climates [1]. In the Kingdom of Saudi Arabia, the electrical energy consumption in the residential sector is almost the same as all other sectors combined [2]. The share of the residential sector in the total electricity consumption in 2006 was 50%, followed by the industrial sector with 23%, the governmental sector (streets, hospitals, mosques and charity associations) with 16%, the commercial sector with 9%, and the agricultural sector with 2% [3,4]. Moreover, a survey of residential-energy consumption in the eastern province of Saudi Arabia indicates that about 75% of the electrical energy consumption was used for space cooling [5]. The Saudi Electricity Company is facing a shortage of electricity during the summer period mainly due to the high usage of electricity in the air conditioning sector [6]. Additionally, the increasing demand for electrical energy in the rapidly expanding towns, cities and industries, greatly exceeds the growth rate of power being made available. Therefore, it is important for local policies to be directed towards replacing traditional refrigeration systems with alternatives operated by sustainable and clean sources of energy in an effort to protect the environment and preserve energy sources.

Energy from the sun is a vast permanent, and plentiful clean energy source. The solar radiation captured by the earth's surface amounts to much higher than the annual global energy use. The energy available from the sun (82×10^{15} W) is about 5200 times greater than the world's needs, as of 2006 [7]. Saudi Arabia, for instance, receives a potent kind of solar radiation because it is located in the heart of one of the world's most affected solar regions [8]. The average annual solar radiation incident on the Arabian Peninsula is about 2200 kW h/m^2 [2,9]. Therefore, harnessing this large amount of energy is extremely beneficial for this part of the world.

Recently, numerous technologies have been industrialized which encourage heat powered cold production systems. Fortunately, solar energy can be used as a driving heat source for these systems. One cooling alternative is the adsorption based cold production technology which is ideally powered by solar radiation. This type of cooling system is recognized to be appropriate and

* Tel.: +966 1 215 7790; fax: +966 1 215 7751.
E-mail addresses: hzahmed@alfaisal.edu, zoheir_hasan@yahoo.com

http://dx.doi.org/10.1016/j.enconman.2015.01.059
0196-8904/© 2015 Elsevier Ltd. All rights reserved.

Nomenclature

A	area (m^2)
C	specific heat ($J\ kg^{-1}\ K^{-1}$)
a	total absorbtance (–)
h	specific enthalpy ($J\ kg^{-1}$)
k	thermal conductivity ($W\ m^{-1}\ K^{-1}$)
N_u	Nusselt number (–)
m	mass (kg)
P	pressure (Pa)
P_r	Prandtl number (–)
$\dot{Q}$	heat (W)
q_{sh}	sorption heat ($W\ kg^{-1}$)
R	thermal resistance ($K\ W^{-1}$)
R_a	Rayleigh number (–)
$\dot{S}$	solar radiation ($W\ m^{-2}$)
T	temperature (K)
t	time (s)
u	specific internal energy ($J\ kg^{-1}$)
U	coefficient of convection ($W\ m^{-2}\ K^{-1}$)
$\forall_b$	bed volume (m^3)
V	velocity ($m\ s^{-1}$)
X	concentration ratio ($kg\ kg^{-1}$)

Greek letters

β	collector-bed tilt angle (deg.)
ρ	density ($kg\ m^{-3}$)
ε	bed porosity (–)
δ	thickness (m)
λ	adsorber surface density ($kg\ m^{-2}$)
σ	Stefan–Boltzmann constant ($W\ m^{-2}\ K^{-4}$)
ϵ	emissivity (–)
θ	adsorbate volume fraction (–)
ζ	solar capturing index (–)
ξ	solar-to-cold conversion factor (–)
η	efficiency (–)

Subscripts

∞	ambient
a	adsorbate phase
con	condenser
eV	evaporator
g	gas phase
ab	absorber plate
ad	adsorber
b	beam
c	glass cover
d	diffuse
eff	effective
dp	dew point
r	reflected
loss	losses
sky	sky
s	solid medium, saturation
tot	total
u	useful

Abbreviations

COP	coefficient of performance
SCOP	solar coefficient of performance
SCP	specific cooling power
SAR	solar adsorption refrigeration

relevant for freezing, refrigeration, and air conditioning applications. Furthermore, adsorption based cooling systems operate with naturally benign refrigerants which have zero ozone depleting potential. As well, adsorption refrigeration systems are regarded as simple control machines and the absence of corrosion and vibration matter is an attractive feature for these types of systems. Additionally, the heat source temperatures that can be used, could be as low as 50 °C, which marks these systems as very attractive when driven by solar energy [10]. However, the dependency on the presence of the radiation from the sun makes these machines intermittent in operation. There has been extensive research and studies on the intermittent solar-driven adsorption refrigeration system [11–21]. The flat configuration adsorption bed ice maker [22–24] and the tubular configuration of the adsorber-collector integration [7,25,26] were studied and discussed. Furthermore, the concentrated solar collector was investigated to power the system as well [27–32].

The performance and operation of the intermittent solar-driven adsorption cooling system depends on several factors which include the climatic conditions and the system design parameters. One of these design parameters is the adsorber surface density which is defined as the mass of the adsorbent per unit area of the solar collector. The adsorber surface density is a major parameter, which is strongly coupled with the other design parameters and climatic conditions. This factor causes a considerable impact on the behaviour, performance, and operation of the intermittent SAR system. Therefore, the current work is devoted to explore the dependency of the intermittent SAR system operation and performance on the adsorber surface density.

2. The intermittent SAR system description

The intermittent SAR system consists of a solar collector-bed integration, condenser, evaporator, refrigerant tank, throttling device, and non-return valves, Fig. 1. The collector-bed integration module has a glass covering at the top and is well insulated from the lateral surfaces as well as from the bottom surface. An absorber plate is attached to the top of the adsorption reactor, which

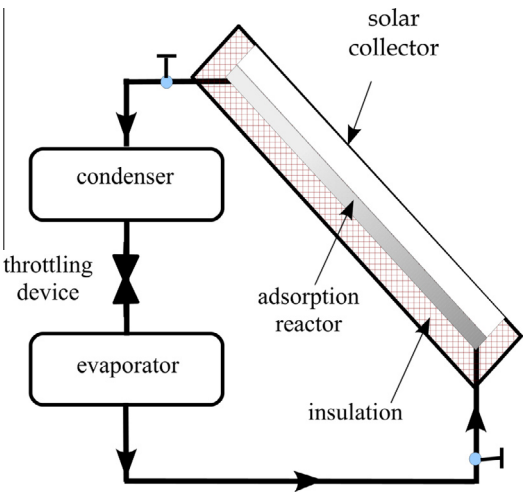

Fig. 1. Illustration of the intermittent solar-driven adsorption cooling system.

contains the adsorbent-adsorbate pair. Furthermore, the collector-bed set is connected to the condenser and the evaporator through the non-return valves, Fig. 1. The operation of the system as well as the thermodynamic operating cycle are well described and discussed elsewhere [11].

In the present study, an intermittent SAR system which has 1 m^2 surface area and has one glass cover is studied. The system is used as a water chiller and is implemented in Riyadh city, Kingdom of Saudi Arabia (latitude 24.7 N, longitude 46.7 E). The water chiller is investigated on August 25th, 2014 for a complete operating cycle. The adsorption cooler operates with silica gel and water adsorption pair and the collector-bed integration is facing the south and is tilted at an angle of 6° to the horizontal plane. The tilt angle corresponds to the optimum tilt angle of a flat-plate solar collectors installed in Riyadh, during the month of August, according to National Aeronautics and Space Administration (NASA) [33].

3. Mathematical modelling

The developed mathematical representation takes into account the dynamic and transient behaviour of the intermittent SAR system. The adsorption reactor mathematical model is derived based on the coupled mass and energy balance relations. Moreover, the adsorbate thermodynamic properties are calculated from the tabulated values. Furthermore, the solar radiation model is based on the ASHRAE (American Society of Heating, Refrigerating and Air Conditioning Engineers) clear sky model. The real weather conditions (ambient temperature and wind velocity) are taken from the actual hourly recorded data. In addition, the flat plate solar collector is assumed to have one glass cover and is perfectly insulated from the bottom and the lateral sides. The heat capacity effect of the collector and the reactor are considered in the analysis as well.

In the following subsections, the developed mathematical formulations of the intermittent SAR system components and the governing equations are introduced.

3.1. Modelling the solar radiation and weather conditions

The total solar radiation, $\dot{S}_{tot}$, which is accessible to an inclined surface, comprises mainly of three components. The first, which has the largest effect, is the direct beam component, $\dot{S}_b$. The second component is the diffuse solar radiation, $\dot{S}_d$. The third component is the ground reflected solar radiation, $\dot{S}_r$. The calculation procedure of these components, based on the ASHRAE clear sky model, is well explained elsewhere [34]. The total available solar radiation, $\dot{S}_{tot}$, is given by

$$\dot{S}_{tot} = \dot{S}_b + \dot{S}_d + \dot{S}_r \tag{1}$$

However, the actual amount of solar radiation which could be captured by a surface, $\dot{S}$, is less than $\dot{S}_{tot}$ and depends primarily on the optical properties as well as the orientation of the surface relative to the incidence angle of the solar radiation. The amount of solar radiation taken by a surface is expressed by [34]

$$\dot{S} = \mathbf{a}_b\dot{S}_b + \mathbf{a}_d\dot{S}_d + \mathbf{a}_r\dot{S}_r \tag{2}$$

where $\mathbf{a}_b$, $\mathbf{a}_d$, and $\mathbf{a}_r$ are the total absorbtance of the surface for the direct, diffuse, and reflected solar radiation, respectively. In the case of flat plate solar collectors, the absorber surface is commonly covered by one or more covers of glass to trap the infrared radiation and minimize thermal losses from the collector absorber plate. As a result, multiple reflections as well as transmissions are encountered at the interfaces of the cover-plate system. The procedure for calculating the total absorbtance of the surface for the direct, diffuse, and reflected solar radiation is briefly demonstrated elsewhere [23].

The performance and behaviour of the intermittent SAR system during operation is influenced by the immediate changes in the status of its surroundings. These conditions include the ambient temperature T_∞, the velocity of the ambient air V_∞, the air coefficient of convection U_∞, and the sky temperature T_{sky}. Both ambient temperature and air velocity are modelled based on the historical recorded data. Fig. 2 plots the ambient temperature and air velocity changes throughout the day on August 25th, 2014 for Riyadh city in the Kingdom of Saudi Arabia, as recorded by the King Khaled International Airport OERK weather station. The convection coefficient of air is calculated from [35]

$$U_\infty = 5.7 + 3.8V_\infty \tag{3}$$

The effective clear sky temperature is dependent on the ambient air temperature as well as the dew point temperature, T_{dp}, (all in K) and is calculated from Bliss relation as follows [36]

$$T_{sky} = T_\infty\left[0.8 + \frac{T_{dp} - 273}{250}\right]^{0.25} \tag{4}$$

The average dew point temperature is 275 K, according to the previously mentioned records. Consequently, the sky temperature under these conditions equals $T_{sky} = 0.948T_\infty$.

3.2. Glass cover and the absorber plate models

The solar collector and adsorption bed integration, in the present work, consists of one glass cover at the top, and insulation from the bottom and the lateral sides. The collector-bed combination is assumed to be well insulated from the bottom and from the lateral sides. Consequently, the bottom and side heat transfer is extremely small compared to the top heat transfer and can be neglected. Moreover, the system operation has a dynamic and a transient behaviour. Therefore, the heat capacity effect of the system's components is considered in the present analysis. Furthermore, the glass cover and the absorber plate are assumed to have a uniform temperature at T_c and T_{ab}, respectively. Two different conditions of the glass cover and the absorber plate are analysed in the following subsections, corresponding to the two modes of operation; preheating-desorption and precooling-adsorption modes.

3.2.1. Preheating and desorption mode

In this mode of operation, the adsorption bed is being preheated and the adsorbate is being generated from the bed. This mode is powered by the solar radiation. The optical losses from the collector-bed system have been considered previously in Eq. (2). The additional thermal losses and the energy balance equations for the glass cover and the absorber plate are introduced in this subsection. Fig. 3 describes the thermal energy flow through the collector-bed integration and the corresponding thermal resistance circuit during the preheating-generation mode. The energy balance equation for the absorbing plate can be expressed as follows

$$(m_{ab}C_{ab})\frac{dT_{ab}}{dt} = A\dot{S} - \dot{Q}_{ab\to c} - \dot{Q}_u \tag{5}$$

In the above equation, $\dot{Q}_{ab\to c}$ is the heat transferred in the upward direction from the collector absorbing plate towards the glass cover and $\dot{Q}_u$ is the useful heat in the downward direction which is employed to generate the adsorption reactor. $\dot{Q}_{ab\to c}$ accounts for both convection and radiation heat exchanges from the plate to the cover and is determined from

$$\dot{Q}_{ab\to c} = \frac{T_{ab} - T_c}{R^{(rad)}_{ab\to c}} + \frac{T_{ab} - T_c}{R^{(conv)}_{ab\to c}} \tag{6}$$

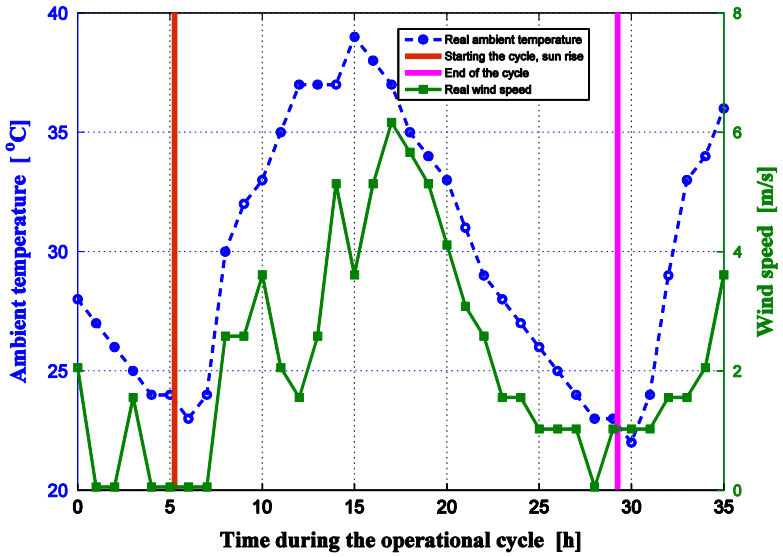

Fig. 2. Ambient temperature and air velocity changes during the operation of the cycle, as recorded by the King Khaled International Airport OERK weather station for Riyadh city on August 25th, 2014.

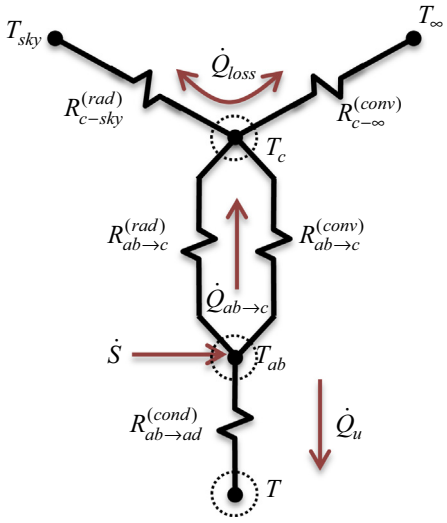

Fig. 3. Schematic representation of the thermal resistance circuit of the collector-reactor combination during the preheating/generation mode.

where $R^{(rad)}_{ab\to c}$ and $R^{(conv)}_{ab\to c}$ are the thermal resistances corresponding to radiation and convection between the plate and the cover, respectively. These resistances are given as follows

$$R^{(rad)}_{ab\to c} = \frac{(1/\epsilon_c) + (1/\epsilon_{ab}) - 1}{\sigma A (T_c + T_{ab})(T_c^2 + T_{ab}^2)} \tag{7}$$

and,

$$R^{(conv)}_{ab\to c} = \frac{\delta_{gap}}{A N_u k_{gap}} \tag{8}$$

where ϵ_c and ϵ_{ab} are the emissivity of the cover and the absorber, respectively. δ_{gap} is the width of the air gap and k_{gap} is the thermal conductivity of the air in the gap. The Nusselt number N_u is calculated from Hollands correlation as follows [34]

$$N_u = 1 + 1.44\left[1 - \frac{1708(\sin 1.8\beta)^{1.6}}{R_a \cos\beta}\right]\left[1 - \frac{1708}{R_a \cos\beta}\right]^{\oplus} + \left[\left(\frac{R_a \cos\beta}{5830}\right)^{1/3} - 1\right]^{\oplus} \tag{9}$$

The notation $(\oplus)$ indicates that if the quantity in the bracket is negative, a zero value should be used. In the above equation, β is the collector-bed tilt angle, and R_a is the Rayleigh number which is given in terms of gap air volumetric coefficient of expansion B, kinetic viscosity υ, and Prandtl number P_r, as follows

$$R_a = \frac{gB(T_{ab} - T_c)\delta^3_{gap} P_r}{\upsilon^2} \tag{10}$$

By considering a linear profile of the temperature distribution in the adsorber, $\dot{Q}_u$ can be found from

$$\dot{Q}_u = \frac{2(T_{ab} - T)}{R_{ab\to ad}} \tag{11}$$

where T is the average temperature of the adsober and $R_{ab\to ad}$ is the adsorber thermal resistance which is calculated from

$$R_{ab\to ad} = \frac{\delta_{ad}}{A k_{eff}} \tag{12}$$

The effective thermal conductivity of the adsorber k_{eff} which includes the effect of the thermal conductivity of the solid k_{sm}, the mobile gas k_g, and the adsorbed phase k_a. The simplest expression for the effective bed conductivity can be found as a volume averaged which is equivalent to the parallel thermal resistances arrangement. This can be written as [37]

$$k_{eff} = k_{sm}(1 - \varepsilon) + k_a\theta + k_g(\varepsilon - \theta) \tag{13}$$

where ε is the porosity of the adsorbent and θ is the adsorbate phase volume faction.

The energy balance for the glass cover can be written as

$$(m_c C_c)\frac{dT_c}{dt} = \dot{Q}_{ab\to c} - \dot{Q}_{loss} \tag{14}$$

The top heat losses in the above equation $\dot{Q}_{loss}$ accounts for the sum of heat losses by convection to the ambient air $\dot{Q}_{c\to\infty}$ and heat exchange by radiation between the cover and the sky $\dot{Q}_{c\to sky}$. This can be expressed as

$$\dot{Q}_{loss} = \dot{Q}_{c\to\infty} + \dot{Q}_{c\to sky} = \frac{T_c - T_\infty}{R^{(conv)}_{c\to\infty}} + \frac{T_c - T_{sky}}{R^{(rad)}_{c\to sky}} \tag{15}$$

where $R^{(rad)}_{c\to sky}$ and $R^{(conv)}_{c\to\infty}$ are given, respectively, by

$$R_{c\to sky}^{(rad)} = [\epsilon_c \sigma A (T_c + T_{sky})(T_c^2 + T_{sky}^2)]^{-1} \quad (16)$$

$$R_{c\to\infty}^{(conv)} = [AU_\infty]^{-1} \quad (17)$$

3.2.2. Precooling and adsorption mode

During the isosteric cooling and the constant pressure adsorption processes, the glass cover is opened to allow the dissipation of the bed heat to the surroundings. The thermal resistance representation for this mode is shown in Fig. 4. In this case, the glass cover behaviour is no longer coupled with the system thermal behaviour. The glass cover and the plate energy balance equations under these conditions are expressed, respectively, by the following expressions

$$(m_c C_c)\frac{dT_c}{dt} = -2\dot{Q}_{loss} \quad (18)$$

and

$$(m_{ab} C_{ab})\frac{dT_{ab}}{dt} = -\dot{Q}_{rej} - \dot{Q}_u \quad (19)$$

The heat rejected from the adsorption reactor $\dot{Q}_{rej}$ is given by

$$\dot{Q}_{rej} = \frac{T_{ab} - T_\infty}{R_{ab\to\infty}^{(conv)}} + \frac{T_{ab} - T_{sky}}{R_{ab\to sky}^{(rad)}} \quad (20)$$

where the thermal resistances $R_{ab\to sky}^{(rad)}$ and $R_{ab\to\infty}^{(conv)}$ are given, respectively, by

$$R_{ab\to sky}^{(rad)} = [\epsilon_c \sigma A (T_{ab} + T_{sky})(T_{ab}^2 + T_{sky}^2)]^{-1} \quad (21)$$

$$R_{ab\to\infty}^{(conv)} = [AU_\infty]^{-1} \quad (22)$$

3.3. Adsorption isotherm and adsorption heat

The adsorption equation of state for the silica gel and water adsorption pair is used to estimate the equilibrium uptake. The S-B-K isotherm model [38–41] is employed in the present work. The S-B-K isotherm model can be expressed by,

$$X = \alpha(T)\left(\frac{P}{P_s(T)}\right)^{\gamma(T)} \quad (23)$$

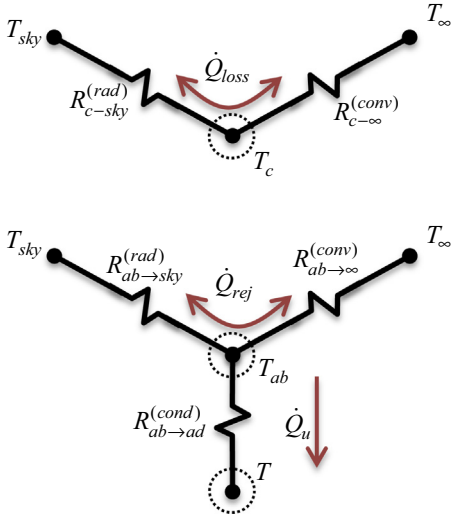

Fig. 4. Schematic representation of the thermal resistance circuit of the cover and the plate during the precooling/adsorption mode.

where

$$\alpha(T) = \sum_{i=0}^{i=3}\alpha_i T^i \text{ and } \gamma(T) = \sum_{j=0}^{j=3}\gamma_j T^j \quad (24)$$

The coefficients α_i and γ_j for the silica gel and water adsorption pair are given in Table 1.

The Clapeyron–Clausius equation is used to calculate the isosteric heat of adsorption or desorption per unit mass of adsorbate as follows

$$q_{sh} = \frac{RT^2}{P}\left[\frac{\partial P}{\partial T}\right]_{X=con} \quad (25)$$

By expressing the pressure explicitly from (23) and performing the partial differentiation, the isosteric heat can be expressed as

$$q_{sh} = -\frac{RT^2}{P}\left[\frac{\tau^{\frac{1}{\gamma(T)}-1}}{[\alpha(T)\cdot\gamma(T)]^2}\right]\left[X^2\cdot\frac{\gamma(T)}{\alpha(T)}\cdot\frac{dP_s(T)}{dT}\cdot\frac{d\alpha(T)}{dT} + \tau\cdot(\ln\tau)\cdot[\alpha(T)]^2\cdot\frac{d\gamma(T)}{dT}\right] \quad (26)$$

where

$$\tau = P_s(T)\cdot\frac{X}{\alpha(T)}$$

The specific enthalpy of the adsorbed refrigerant $h_a(P, T)$ is the difference between the gas phase specific enthalpy $h_g(P, T)$ and the adsorption isosteric heat. It can be found from the following equation

$$h_a(P,T) = h_g(P,T) - q_{sh} \quad (27)$$

Then, the adsorbed phase specific internal energy is calculated from

$$u_a(P,T) = h_a(P,T) - \frac{P}{\rho_a(T)} \quad (28)$$

3.4. Governing equations for the adsorber

The bulk volume of the adsorption bed $\forall_b$ consists of three components; the adsorbent solid, the adsorbate refrigerant phase, and the refrigerant gas phase. The mass contribution of each of these constituents are expressed in terms of the bed total porosity ε and concentration ratio X as follows

$$\begin{aligned}&\text{adsorbent solid mass}: \ m_s = \rho_s(1-\varepsilon)\forall_b\\ &\text{adsorbate phase mass}: \ m_a = Xm_s\\ &\text{gas phase mass}: m_g = \rho_g[\varepsilon - \rho_s(1-\varepsilon)X/\rho_a]\forall_b\end{aligned} \quad (29)$$

The form of the conservation of mass equation for the adsorber relies on the cycle process which the bed undergoes. For the preheating as well as the precooling processes, there is no refrigerant mass transfer into or out of the bed and the mass content of the adsorber is fixed. Consequently, the bed mass balance for these processes is expressed as

$$m_s\frac{dX}{dt} + \forall_b\frac{d}{dt}\left[\varepsilon\rho_g - \frac{\rho_g\rho_s(1-\varepsilon)X}{\rho_a}\right] = 0 \quad (30)$$

Table 1
Coefficients of S-B-K equation for silica gel and water pairs [41].

i,j	α_i	γ_j
0	−6.5314 (kg/kg)	−15.587
1	0.072452 (kg/kg) K^{-1}	0.15915 K^{-1}
2	-0.23951×10^{-3} (kg/kg)K^{-2}	-0.50612×10^{-3} K^{-2}
3	0.25493×10^{-6} (kg/kg) K^{-3}	0.5329×10^{-6} K^{-3}

The corresponding energy conservation equation is given by

$$m_s C_s \frac{d\bar{T}_{ad}}{dt} + m_s \frac{d}{dt}[Xu_a] + \forall_b \frac{d}{dt}\left[\varepsilon\rho_g u_g - \frac{\rho_g \rho_s (1-\varepsilon) X u_g}{\rho_a}\right] = \dot{Q}_u \tag{31}$$

When the bed is connected to the condenser and is isolated from the evaporator during the generation process, the adsorber mass content is reduced by the mass flow rate to the condenser, $\dot{m}_{con}$. Hence, the mass balance and the energy balance are stated in this process, respectively, as

$$m_s \frac{dX}{dt} + \forall_b \frac{d}{dt}\left[\varepsilon\rho_g - \frac{\rho_g \rho_s (1-\varepsilon) X}{\rho_a}\right] = -\dot{m}_{con} \tag{32}$$

and

$$m_s C_s \frac{d\bar{T}_{ad}}{dt} + m_s \frac{d}{dt}[Xu_a] + \forall_b \frac{d}{dt}\left[\varepsilon\rho_g u_g - \frac{\rho_g \rho_s (1-\varepsilon) X u_g}{\rho_a}\right] = \dot{Q}_u - \dot{m}_{con} h_g \tag{33}$$

When the bed is connected to the evaporator and is isolated from the condenser during the adsorption process, the bed mass content increases at a rate of $\dot{m}_{eV}$. Then, the mass balance equation is given by

$$m_s \frac{dX}{dt} + \forall_b \frac{d}{dt}\left[\varepsilon\rho_g - \frac{\rho_g \rho_s (1-\varepsilon) X}{\rho_a}\right] = \dot{m}_{eV} \tag{34}$$

The energy balance is given by

$$m_s C_s \frac{d\bar{T}_{ad}}{dt} + m_s \frac{d}{dt}[Xu_a] + \forall_b \frac{d}{dt}\left[\varepsilon\rho_g u_g - \frac{\rho_g \rho_s (1-\varepsilon) X u_g}{\rho_a}\right] = \dot{Q}_u + \dot{m}_{eV} h_{eV} \tag{35}$$

3.5. Performance indices

The performance indices which are used in the present work to evaluate the intermittent SAR system operation include the solar capturing index ζ, solar-to-cold conversion factor ξ, solar coefficient of performance SCOP, the adsorber surface density λ, and others. The solar capturing index is defined as the fraction of the total solar energy available during the reactor heating period from the total solar energy available during the daylight time period. This parameter specifies the system capacity to use as much as possible the accessible solar radiation during the day. The solar capturing index is expressed as follows

$$\zeta = \left(\int_{t_1}^{t_3} \dot{S}_t(t)dt\right) \Big/ \left(\int_{t_{sr}}^{t_{ss}} \dot{S}_t(t)dt\right) \tag{36}$$

The solar-to-cold conversion factor ξ is another important parameter which indicates the system capability to produce useful output (cooling effect at the evaporator side) from the existing in hand resources (the total available solar radiation during the day). This can be expressed mathematically by

$$\xi = \left(\int_{t_4}^{t_1} \dot{Q}_{eV}(t)dt\right) \Big/ \left(A \int_{t_{sr}}^{t_{ss}} \dot{S}_t(t)dt\right) \tag{37}$$

The solar coefficient of performance is given in terms of the COP and the total efficiency of the collector η_c (which includes thermal and optical losses effect), as follows

$$\text{SCOP} = \eta_c \times \text{COP} = \left(\int_{t_4}^{t_1} \dot{Q}_{eV}(t)dt\right) \Big/ \left(A \int_{t_1}^{t_3} \dot{S}_t(t)dt\right) \tag{38}$$

where,

$$\text{COP} = \left(\int_{t_4}^{t_1} \dot{Q}_{eV}(t)dt\right) \Big/ \left(\int_{t_1}^{t_3} \dot{Q}_u(t)dt\right) \tag{39}$$

and,

$$\eta_c = \left(\int_{t_1}^{t_3} \dot{Q}_u(t)dt\right) \Big/ \left(A \int_{t_1}^{t_3} \dot{S}_t(t)dt\right) \tag{40}$$

The solar-to-cold conversion factor can be expressed in terms of the solar capturing index and the solar coefficient of performance as follows

$$\xi = \zeta \times \text{SCOP} = \zeta \times \eta_c \times \text{COP} \tag{41}$$

The adsorber surface density λ is the mass of the adsorbent per unit area of the collector absorber plate and is given by

$$\lambda = \frac{m_s}{A} \tag{42}$$

Another performance parameter which is commonly used for SAR system performance evaluation is the specific cooling power (SCP). The SCP is the cooling power per unit mass of adsorbent and is expressed by

$$\text{SCP} = \frac{\int_{t_4}^{t_1} \dot{Q}_{eV}(t)dt}{24 \times 3600 \times m_s} \tag{43}$$

4. Results and discussion

Based on the previously discussed mathematical dynamic simulation model, a Matlab computer program is developed to run the system simulation. The simulation model resulted in a differential coupled nonlinear system of equations. This system of equations is solved by the 4th order Runge–Kutta method. Additionally, the thermodynamic properties of the water as a refrigerant and the air existing in between the glass cover and the absorber plate are determined based on their tabulated values. The partial derivatives of the adsorbate and gas phases of water properties are calculated by using the high accuracy finite difference approximation method for derivatives which is described in [42]. Several runs of the computer code are performed in order to determine the system performance corresponding to the variations of the surface density. Each run represents a complete cycle of the intermittent SAR system with the same design parameters and conditions but with a different value of the surface density. Furthermore, Table 2 lists the values of various parameters which are used in the simulation and are found in the mathematical model.

Fig. 2 shows the values of ambient temperature and air velocity which are manipulated to simulate the operation of the cycle. Fig. 5 plots the three components of the solar radiation; direct beam $\dot{S}_b$, sky diffuse $\dot{S}_d$, and ground reflected components $\dot{S}_r$, based on the clear sky model for Riyadh city during the simulation day on August 25th, 2014. The total available solar radiation $\dot{S}_{tot}$ is shown as well. The ground reflected component is found to be nearly zero because the collector-bed tilt angle is very small, 6° from the horizontal plane. Furthermore, the daylight period during the simulation day is 12.64 h which starts at 5.67 AM and ends at 6.32 PM.

The impact of the adsorber surface density on the system dynamic behaviour and operation is explained in Fig. 6 through Fig. 9. In these figures, two cases are pronounced. The first case is related to a normal operation of the system in which the intermittent SAR machine successfully completes the four processes of the cycle and produces cooling effect at the evaporator, Figs. 6 and 7. The second case refers to the unusual operation of the cycle in which the adsorption cooler fails to complete the cycle and hence no cooling effect is noticed at the evaporator, Figs. 8, 9.

Table 2
The parameters used in the simulation.

Symbol	Parameter	Value
Cycle design parameters		
T_{eV}	Evaporator temperature	10 °C
T_{con}	Condensation temperature	40 °C
Adsorbent (Silica gel)		
ρ_s	Particle density of the adsorbent	700 kg m^{-3}
C_s	Specific heat of the adsorbent	820 J kg^{-1} K^{-1}
ε	Bed total porosity	0.4
k_s	Thermal conductivity of the adsorbent	0.198 W m^{-1} K^{-1}
Solar collector parameters		
β	Collector-bed tilt angle	6 deg.
A_{ab}	Absorber plate surface area	1 m^2
ρ_{ab}	Density of the absorber plate (stainless steel)	7850 kg m^{-3}
C_{ab}	Specific heat of the absorber plate (stainless steel)	500 J kg^{-1} K^{-1}
t_{ab}	Absorber plate thickness	3 mm
ϵ_{ab}	Emissivity of the absorber plate (black chrome selective coating)	0.05
α_{ab}	Absorptivity of the absorber plate	0.95
δ_{gap}	Air gap width between the plate and the cover	10 cm
$\mathscr{C}_c$	Specific heat of the glass cover	820 J kg^{-1} K^{-1}
ρ_c	Density of the glass cover	2515 kg m^{-3}
δ_c	Glass cover thickness	3 mm
ϵ_c	Emissivity of the glass cover	0.88

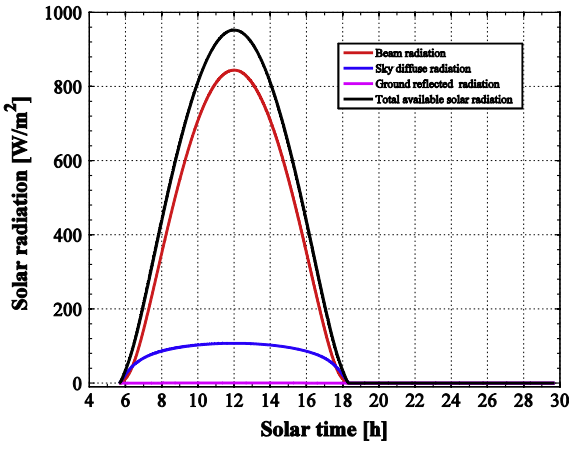

Fig. 5. Solar radiation components for Riyadh city, August 25th, 2014.

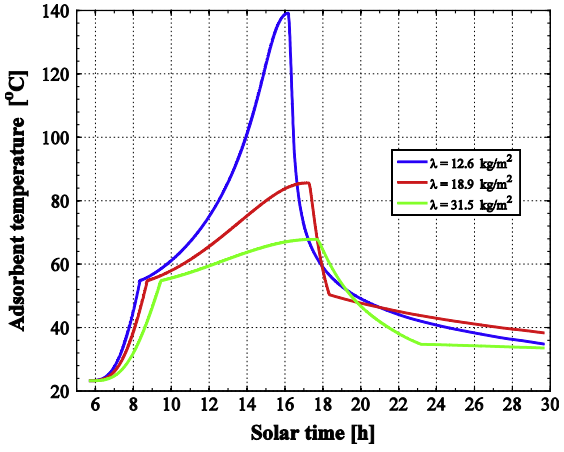

Fig. 7. Reactor temperature development at different values of surface densities for the normal operation cycles.

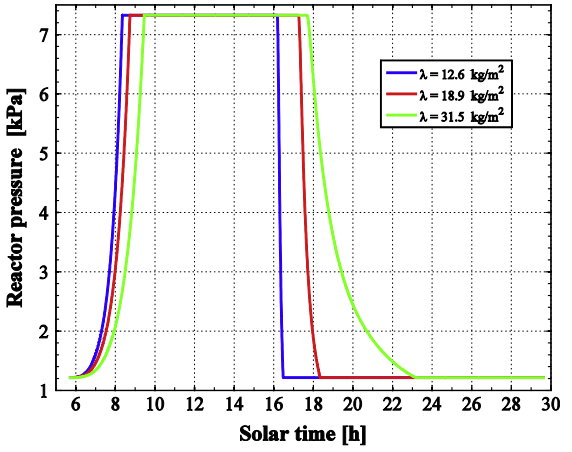

Fig. 6. Reactor pressure development at different values of surface densities for the normal operation cycles.

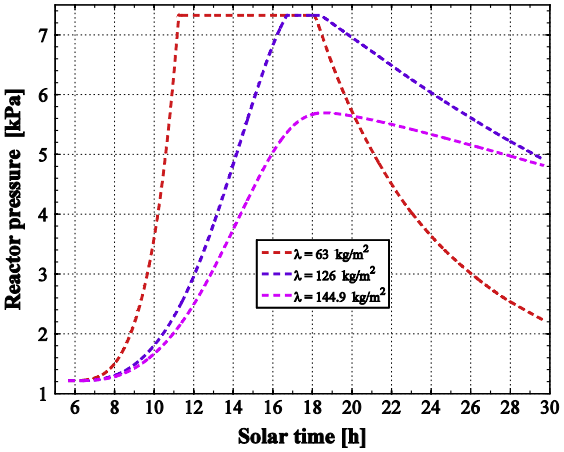

Fig. 8. Reactor pressure development at different values of surface densities for the non-working cycles.

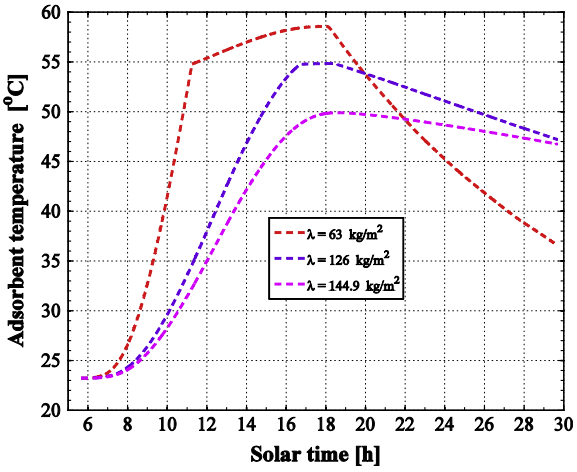

Fig. 9. Reactor temperature development at different values of surface densities for the non-working cycles.

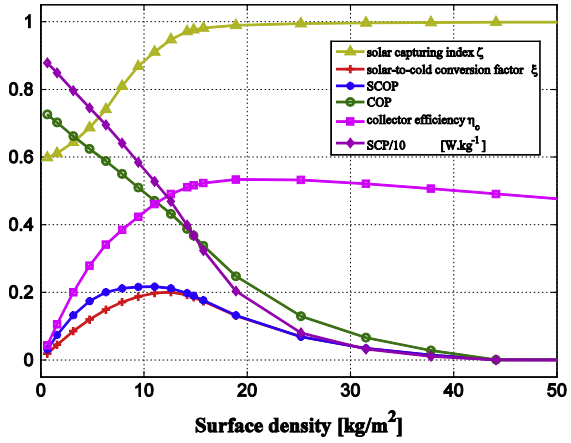

Fig. 10. Variation of the system performance indices with the surface density.

The development of the reactor pressure and temperature corresponding to different values of surface densities for a number of successfully completed operating cycles is depicted in Figs. 6 and 7, respectively. In all cycles, the reactor pressure elevates from the evaporator pressure, which corresponds to an evaporator temperature of 10 °C, to the condenser pressure, which corresponds to a condensation temperature of 40 °C. As expected, cycles with low values of λ are activated faster and they reach the generation temperature, 54.7 °C, and the condenser pressure, 7.3 kPa, more rapidly compared with cycles having large λ values, Figs. 6 and 7. Furthermore, the cycle maximum temperature at the end of the desorption-condensation process is higher for the low λ systems. This means lower values of the cycle concentration ratio at the end of desorption phase. Therefore, systems having low surface densities are expected to attain higher values of their COP. Moreover, low λ systems show a rapid response to the precooling process and therefore an early start of the adsorption-evaporation phase, as shown in Fig. 6 and 7. This allows the low λ adsorption beds to adsorb more refrigerant vapour per unit adsorbent mass. Consequently, higher cooling effect per unit adsorbent mass, and hence higher COP, is expected for the low λ systems in comparison with those having higher λ.

Figs. 8 and 9 plot the evolution of pressure and temperature, respectively, for a number of massive SAR systems at different values of λ. All the cases shown in these graphs fail to complete the thermodynamic cycle and no cooling effect is noticed at the evaporator side. One of the shown cases ($\lambda = 63$ kg/m^2) ends the desorption-condensation phase at low final temperature, about 59 °C, and hence small amount of desorbed refrigerant is moved towards the condenser. However, this case fails to reach the evaporator pressure till the end of the cycle. The reason is the large amount of thermal energy stored in the adsorber which is slowly dissipated to the surroundings. Besides, the deterioration of the heat transfer coefficient inside the adsorption reactor when λ increases due to the thick adsorbent layer. Another studied case with $\lambda = 144.9$ kg/m^2 fails to reach the desorption temperature and the condenser pressure, as shown in Figs. 8 and 9. That is because this case requires large amount of thermal energy, which is not provided by the solar radiation, to reach the activation state. As a result, the condenser has not received any refrigerant mass during the system operation.

The influence of the surface density on the overall system performance indices is illustrated in Fig. 10. It is noticed that, SAR systems with lower surface densities show higher values of the COPs compared with those systems having bulky beds. This is because of the high level of maximum cycle temperature and low level of the minimum concentration ratio of the low λ beds compared with the high λ beds. That is besides the fast response to heating and cooling in case of low λ reactors. It is also noticed that SAR machines with λ value greater than 44 kg/m^2 will fail in operation and will not produce cooling energy (COP = 0). The collector total efficiency shows an increasing trend as λ increases. That is due to the decreased thermal losses from the collector plate, which is at low level of temperatures, in case of high λ values. The resultant effect of the COP and the collector total efficiency gives the profile of the SCOP as illustrated in Fig. 10. It is also found that, the values of SCP show a continuous decreasing profile as the surface density increases. This is due to the deterioration of the adsorption and desorption capacity of the bed by the increase in the adsorbent thickness. In other words, adsorbent layers near the absorber plate (top adsorbent layers) have good heat transfer and attain a higher level of refrigerant adsorption/desorption capability compared with other deeper layers (bottom adsorbent layers) which have poor heat transfer. Moreover, top adsorbent layers show a more rapid response to the generation/precooling processes compared to the bottom adsorbent layers. Therefore, adsorbent layers near the absorber plate acquire higher/lower temperature at the end of the desorption/adsorption process compared to other deeper adsorbent layers. As a consequence, the amount of refrigerant vapour which is generated from the top adsorbent layers is larger than that generated from the bottom adsorbent layers per unit mass of adsorbent. Consequently, higher cooling effect per unit adsorbent mass, and hence higher SCP, is expected for the low surface density systems in comparison with those systems having higher values of surface density. Low λ adsorption beds reach the end of generation-condensation phase earlier before the sunset time compared with the higher λ beds, as plotted in Figs. 6 and 7. This indicates the poor ability of the low λ systems to capture the available solar energy. In other words, large amount of the available solar radiation is not used by the low λ adsorbers and therefore low solar capturing index ζ is expected for these systems, as shown in Fig. 10. Moreover, the efficiency of the intermittent SAR machine to use the available solar radiation and produce cold is plotted in Fig. 10 in terms of the solar-to-cold conversion factor ξ. Although low λ systems attain high COPs, their solar-to-cold conversion factor is low due to the low solar capturing index. Consequently, the COP is not the exact indicator for the SAR system performance and the solar-to-cold conversion factor is recommended when designing SAR systems. Additionally, there is a peak value for the solar-to-cold conversion factor at about 0.2 corresponding to a certain value of $\lambda = 12.6$ kg/m^2, as illustrated in

Fig. 10. Although the corresponding value of the cycle COP equals 0.43, which is not the maximum, this case is considered the optimum design point for the SAR system under the conditions of the studied case.

5. Conclusion

In the present work, a theoretical study on the effect of the adsorber surface density on the performance of the intermittent solar-driven adsorption cooling system is introduced. The mathematical formulations of different components of the intermittent SAR system are developed. A computer code is developed in Matlab to run the simulations and determine the system performance.

The obtained results show two cases of operation. The first is a normal operation in which the SAR system successfully completes the four processes of the cycle and produces cooling effect at the evaporator. The second case is the unusual operation of the cycle in which the cooler fails to complete the cycle and to produce cooling effect. It is also shown that the studied SAR machine will fail in operation and will not produce cold (COP = 0) for λ value greater than 44 kg/m^2. Moreover, the COP and the SCP increase with decreasing surface density. Additionally, the optimum solar-to-cold conversion factor attains a value of 0.2 corresponding to surface density of 12.6 kg/m^2 and COP of 0.43. The work done showed that the COP is not the precise measure for the SAR system performance. The solar-to-cold conversion factor is recommended when designing SAR systems.

Acknowledgements

The authors of this paper would like to thank Alfaisal University, Riyadh, Kingdom of Saudi Arabia for providing the support to complete this work. The present study is accomplished under the Internal Research Grant IRG2014 Project No. 208260101147.

References

[1] Hassan HZ, Mohamad AA. A review on solar cold production through absorption technology. Renew Sustain Energy Rev 2012;16:5331–48.
[2] Hepbasli A, Alsuhaibani Z. A key review on present status and future directions of solar energy studies and applications in Saudi Arabia. Renew Sustain Energy Rev 2011;15:5021–50.
[3] Al-Ajlan SA, Al-Ibrahim AM, Abdulkhaleq M, Alghamdi F. Developing sustainable energy policies for electrical energy conservation in Saudi Arabia. Energy Policy 2006;34:1556–65.
[4] Al-Hadhrami LM, Ahmad A. Assessment of thermal performance of different types of masonry bricks used in Saudi Arabia. Appl Therm Eng 2009;29:1123–30.
[5] Al-Sulaiman FA, Zubair SM. A survey of energy consumption and failure patterns of residential air-conditioning units in Eastern Saudi Arabia. Energy 1996;21:967–75.
[6] Hasnain SM, Alabbadi NM. Need for thermal-storage air-conditioning in Saudi Arabia. Appl Energy 2000;65:153–64.
[7] Hassan HZ, Mohamad AA, Bennacer R. Simulation of an adsorption solar cooling system. Energy 2011;36:530–7.
[8] Alnatheer O. The potential contribution of renewable energy to electricity supply in Saudi Arabia. Energy Policy 2005;33:2298–312.
[9] Alawaji SH. Evaluation of solar energy research and its applications in Saudi Arabia — 20 years of experience. Renew Sustain Energy Rev 2001;5:59–77.
[10] Wang RZ, Oliveira RG. Adsorption refrigeration—an efficient way to make good use of waste heat and solar energy. Prog Energy Combust Sci 2006;32:424–58.
[11] Hassan HZ, Mohamad AA. A review on solar-powered closed physisorption cooling systems. Renew Sustain Energy Rev 2012;16:2516–38.
[12] Wang RZ, Li M, Xu YX, Wu JY. An energy efficient hybrid system of solar powered water heater and adsorption ice maker. Sol Energy 2000;68:189–95.
[13] Leite APF, Daguenet M. Performance of a new solid adsorption ice maker with solar energy regeneration. Energy Convers Manag 2000;41:1625–47.
[14] Hassan HZ. Effect of parameters variation on the performance of adsorption based cooling systems. Int Rev Mech Eng 2013;7:24–37.
[15] Hassan HZ. Energy analysis and performance evaluation of the adsorption refrigeration system. ISRN Mech Eng 2013.
[16] Ogueke NV, Anyanwu EE. Design improvements for a collector/generator/adsorber of a solid adsorption solar refrigerator. Renew Energy 2008;33:2428–40.
[17] Zhao H, Zhang M, Zhenyan L, Yanling L, Xiaodong M. Mechanical and experimental study on freeze proof solar powered adsorption cooling tube using active carbon/methanol working pair. Energy Convers Manag 2008;49:2434–8.
[18] Critoph RE. Performance limitations of adsorption cycles for solar cooling. Sol Energy 1988;41:21–31.
[19] Hassan HZ, Mohamad AA, Al-Ansary HA. Development of a continuously operating solar-driven adsorption cooling system: thermodynamic analysis and parametric study. Appl Therm Eng 2012;48:332–41.
[20] Jing H, Exell RHB. Simulation and sensitivity analysis of an intermittent solar-powered charcoal/methanol refrigerator. Renew Energy 1994;4:133–49.
[21] Anyanwu E, Oteh U, Ogueke N. Simulation of a solid adsorption solar refrigerator using activated carbon/methanol adsorbent/refrigerant pair. Energy Convers Manag 2001;42:899–915.
[22] Li M, Wang R, Xu Y, Wu J, Dieng A. Experimental study on dynamic performance analysis of a flat-plate solar solid-adsorption refrigeration for ice maker. Renew Energy 2002;27:211–21.
[23] Hassan HZ. Development of a solar-driven adsorption cooling system for a continuous production of cold. University of Calgary, 2012.
[24] Hassan HZ. A solar powered adsorption freezer: a case study for Egypt's Climate. Int J Energy Eng 2013;3:21–9.
[25] Chekirou W, Chikouche A, Boukheit N, Karaali A, Phalippou S. Dynamic modelling and simulation of the tubular adsorber of a solid adsorption machine powered by solar energy. Int J Refrig 2014;39:137–51.
[26] Hildbrand C, Dind P, Pons M, Buchter F. A new solar powered adsorption refrigerator with high performance. Sol Energy 2004;77:311–8.
[27] Abu-Hamdeh NH, Alnefaie KA, Almitani KH. Design and performance characteristics of solar adsorption refrigeration system using parabolic trough collector: experimental and statistical optimization technique. Energy Convers Manag 2013;74:162–70.
[28] Lu ZS, Wang RZ, Xia ZZ, Lu XR, Yang CB, Ma YC, et al. Study of a novel solar adsorption cooling system and a solar absorption cooling system with new CPC collectors 2013:50.
[29] Alam KCA, Saha BB, Akisawa A. Adsorption cooling driven by solar collector: a case study for Tokyo solar data. Appl Therm Eng 2013;50:1603–9.
[30] Umair M, Akisawa A, Ueda Y. Performance evaluation of a solar adsorption refrigeration system with a wing type compound parabolic concentrator 2014:1448–66.
[31] González MI, Rodríguez LR. Solar powered adsorption refrigerator with CPC collection system: collector design and experimental test. Energy Convers Manag 2007;48:2587–94.
[32] El Fadar A, Mimet A, Azzabakh A, Pérez-García M, Castaing J. Study of a new solar adsorption refrigerator powered by a parabolic trough collector. Appl Therm Eng 2009;29:1267–70.
[33] NASA. National Aeronautics and Space Administration (NASA): Surface Meteorology and Solar Energy. <https//eosweb.larc.nasa.gov/cgi-Bin/sse/grid.cgi?email=skip@larc.nasa.gov>, Date Accessed Oct 4th, 2014 2014.
[34] Duffie JA, Beckman WA. Solar Engineering of Thermal Processes. 4th Ed. Wiley, 2013.
[35] Saraf GR, Hamad FAW. Optimum tilt angle for a flat plate solar collector. Energy Convers Manag 1988;28:185–91.
[36] Bliss RW. Atmospheric radiation near the surface of the ground: a summary for engineers. Sol Energy 1961;5:103–20.
[37] Kaviany M. Principles of heat transfer in porous media. New York: Springer; 1995.
[38] Saha B, Boelman E, Kashiwagi T. Computer simulation of a silica gel-water adsorption refrigeration cycle- the influence of operating conditions on cooling output and COP. ASHRAE TRANS 1995;101:348–57.
[39] Habib K, Saha BB, Koyama S. Study of various adsorbent–refrigerant pairs for the application of solar driven adsorption cooling in tropical climates. Appl Therm Eng 2014:1–9.
[40] Wang D, Zhang J, Yang Q, Li N, Sumathy K. Study of adsorption characteristics in silica gel–water adsorption refrigeration. Appl Energy 2014;113:734–41.
[41] Chua HT, Ng KC, Malek A, Kashiwagi T, Akisawa A, Saha BB. Modeling the performance of two-bed, sillica gel-water adsorption chillers. Int J Refrig 1999;22:194–204.
[42] Hassan HZ, Mohamad AA, Atteia GE. An algorithm for the finite difference approximation of derivatives with arbitrary degree and order of accuracy. J Comput Appl Math 2012;236:2622–31.